Mon. Not. R. Astron. Soc. **362,** 66–78 (2005) doi:10.1111/j.1365-2966.2005.09265.x

Multicolour high-speed photometry of the subdwarf B star PG 0014+067 with ULTRACAM★

C. S. Jeffery,[1]† C. Aerts,[2,3] V. S. Dhillon,[4] T. R. Marsh[5] and B. T. Gänsicke[5]

[1]*Armagh Observatory, Armagh BT61 9DG*
[2]*Institute of Astronomy, Catholic University of Leuven, Celestijnenlaan 200 B, B - 3001 Leuven, Belgium*
[3]*Department of Astrophysics, University of Nijmegen, PO Box 9010, 6500 GL Nijmegen, the Netherlands*
[4]*Department of Physics and Astronomy, University of Sheffield, Sheffield S3 7RH*
[5]*Department of Physics, University of Warwick, Coventry CV4 7AL*

Accepted 2005 May 23. Received 2005 May 6; in original form 2005 April 5

ABSTRACT

The non-radially pulsating subdwarf B star PG 0014+067 has previously been presented as a classic case for asteroseismological study, having a moderately rich mode spectrum uncomplicated by severe rotational splitting. Notwithstanding the excellence of previous work, empirical evidence for mode identification is needed to test the modelling results. Consequently high-speed multicolour photometry was obtained over six nights in 2004 August using the high-speed multichannel photometer ULTRACAM on the 4.2-m William Herschel Telescope with a sampling interval of 5 s. To ameliorate the window function, additional single-channel photometry was obtained on five nights in the same time envelope using the 2-m Faulkes Telescope North with a sampling interval of 23 s. 19 individual frequencies have been identified in a combined 'white light' data set. Amplitudes have been measured in filtered light (u', g' and r') for 13 of these. Three groups of closely spaced frequencies have spacings of 3, 13 and 2 μHz. Although on the cusp of the frequency resolution, there is evidence that the rotational period should be nearer to 4 d rather than the 1.35 d reported previously, if we assume that these close frequencies belong to a multiplet. It has not proved possible to identify modes unambiguously using the amplitude ratio method because of the errors on the amplitudes, but we do exclude that the two dominant modes have $l = 3$ or 4; they must be either $l = 0$, 1, 2.

Key words: stars: individual: PG 0014+067 – stars: interiors – stars: oscillations – subdwarfs – stars: variables: other.

1 INTRODUCTION

Since the discovery of non-radial pulsations in subdwarf B (sdB) stars (Kilkenny et al. 1997), much effort has been directed towards asteroseismological studies of their internal structure (e.g. Brassard et al. 2001; Kilkenny et al. 2002, 2003). Such effort is justified in view of their significant roles in populations of evolved stars (D'Cruz et al. 2000) and in the late evolution of close binary stars (Han et al. 2002, 2003).

Primarily manifest as multiperiodic light variations with periods of 100–500 s, these pulsations have also been measured in colour (Koen 1998), radial velocity (Jeffery & Pollacco 2000; O'Toole et al. 2000) and line strength (O'Toole et al. 2003). Jeffery et al. (2004) have shown how, with a 4-m telescope and a multicolour high-speed photometer, colour variations may be used to identify the spherical degree of the principal modes of two pulsating sdB stars, KPD 2109+4401 and HS 0039+4302.

Subdwarf B stars are helium-core burning stars with a total mass $M \sim 0.5$ M$_\odot$ and a very thin hydrogen-rich envelope ($M_e \sim 0$–0.01 M$_\odot$; Heber 1986). Short-period pulsations are driven in approximately 10 per cent of sdBs by the κ-mechanism, mediated by Fe-group abundances (Charpinet et al. 1996) enhanced in the driving zone by selective diffusion (Charpinet et al. 1997). The ultimate goal of an asteroseismological study is to measure M, M_e and the chemical stratification directly. This represents a major challenge. Diffusion produces a complex chemical stratification, which is superimposed on the chemical profile of the envelope at core helium ignition. The latter is not trivial to determine, particularly for such low-mass envelopes, because it carries its history from the H-burning shell of the red giant progenitor. The situation may be further complicated if the star rotates, if it rotates differentially, or if it possesses a significant magnetic field.

★Based on observations obtained with the William Herschel Telescope operated on the island of La Palma by the Isaac Newton Group in the Spanish Observatorio del Roque de los Muchachos of the Instituto de Astrofisica de Canarias, and on observations obtained with Faulkes Telescope North on the island of Maui, Hawaii, operated by the Faulkes Telescope Project.

†E-mail: csj@arm.ac.uk

To resolve so many unknowns, asteroseismology requires a subject with a rich pulsation spectrum and modes probing many layers at different depths. The two targets already studied by us, KPD 2109+4401 and HS 0039+4302, are relatively poor in respect to the number of frequencies detected – although more sensitive studies are certain to detect more.

Detailed asteroseismic analyses have been reported for only two pulsating sdBs, namely PG 0014+067 (Brassard et al. 2001; Charpinet et al. 2005a) and PG 1219+534 (Charpinet et al. 2005b,c), with 16 and 12 positively identified frequencies, respectively. The first study of PG 0014+067 (Brassard et al. 2001) was seminal in demonstrating the power of asteroseismology in probing sdB star structure and evolution; the accuracy of the mass measurement and its agreement with canonical stellar evolution predictions have given impetus to the entire field. However, the number and values of observed frequencies appear to require either high values of spherical degree l or splitting of the frequency-degenerate m-modes through rapid rotation (Kawaler & Hostler 2004, 2005).

While it has been argued that models with $l \geqslant 3$ should be difficult to observe photometrically, our own observations have clearly shown $l = 4$ modes present in KPD 2109+4401 and HS 0039+4302 (Jeffery et al. 2004). This is not unexpected, for the visibility b_l of even modes is known to fall off less steeply ($b \propto l^{-2.5}$) than that of odd modes ($b \propto l^{-3.5}$; Balona & Dziembowksi 1999). Nevertheless, the apparently slow surface rotation of most sdB stars may mask a more rapidly rotating core (Sills & Pinsonneault 2000), which may give rise to differential splitting between the frequencies of modes of different radial order k (Kawaler & Hostler 2004, 2005). The two exceptions are PG 1605+072, with $v \sin i = 31$ km s^{-1} (Heber, Reid & Werner 2000a) and KPD 1930+2752, which is likely to be a fast rotator because of its short orbital period (Billères et al. 2000). A recurrent spacing of ~9 μHz between closely spaced frequencies in PG 0014+067 has already been reported (Brassard et al. 2001).

2 OBSERVATIONS

In order to address the questions outlined above, the Whole Earth Telescope (WET) adopted PG 0014+067 as its principal target for its campaign in the autumn of 2004 (Xcov24). The goal of these observations would be to resolve rotationally split multiplets by improving the frequency resolution. At 16 mag, PG 0014+067 would represent a challenging target for the WET and so the authors applied for time on the 4.2-m William Herschel Telescope (WHT) both to augment the WET campaign and to obtain multicolour information that would help to identify pulsation modes. Six WHT nights were allocated to this project in 2004 August. The vagaries of telescope scheduling prevented any overlap with the WET run scheduled for 2004 October. In partial mitigation, 14 h on the 2.0-m Faulkes Telescope North (FTN) were kindly made available by the Faulkes Telescopes team, providing a stress test for the newly commissioned telescope. The latter observations were supported by tests of timing accuracy and photometric stability, which were carried out as summer projects by local high school students (O'Leary 2004; Quinn 2004).

This paper describes results obtained from the WHT and FTN data alone. However, it is emphasized that the data would probably not have been obtained without the motivation provided by the WET campaign. Both teams worked closely in preparation of the telescope applications and in execution of the observations. For example, the PI (Kawaler) for the WET campaign was promptly sent the quick-look white light curve from the WHT, while one of us (Aerts) was present at the WET headquarters shortly after the WET campaign. So while the current data and the WET data are independent of one another, the results they demonstrate in common represent a mutual effort.

2.1 William Herschel Telescope

Observations were made with the WHT on 2004 August 20, 21, 22, 23, 24 and 25 using the high-speed three-channel photometer ULTRACAM (Dhillon et al., in preparation). The Sloan filters u', g' and r' (Fukugita et al. 1996) were used, one in each of the three cameras. Conditions on the first two nights were excellent, with seeing below 0.4 arcsec and no moon. Regrettably, approximately 3 h of observing time was lost due to a short circuit associated with observing at very low elevations. This was traced and eliminated by August 22. Subsequent nights were increasingly affected by poorer seeing, higher humidity, some cloud and moonlight. A summary of the observations is provided in Table 1.

Each ULTRACAM camera is capable of observing a 5 × 5 arcmin^2 field of view. The time taken to read out each science frame depends on the fraction of the frame required for subsequent analysis. To achieve millisecond exposures, ULTRACAM must be operated with very small windows. Exposure times are also dictated by the need to avoid saturating any stellar image in any frame. Because a temporal resolution of a few seconds is sufficient for studying pulsating sdB stars, approximately half of the chip was used to obtain 5-s exposures without image saturation. The dead time between exposures, due to frame transfer, was 24 ms.

To allow good differential photometry, the chip was oriented and windowed to include five potential comparison stars in the relatively sparse field around PG 0014+067. Details are given in Table 2 and Fig. 1, including magnitudes relative to the target (V) obtained from the ratios of mean counts with the star close to the meridian. In all, just over 60 000 usable science frames were recorded.

Table 1. Journal of ULTRACAM observations in 2004 August.

UT start	UT end	$t_{\rm exp}$/s	$n_{\rm exp}$
2004 Aug 21 01:33	21 06:04	5	3216
22 00:20	22 06:14	5	4353
22 23:24	23 06:02	5	4745
23 23:30	24 05:57	5	3726
25 03:02	25 06:00	5	1942
25 23:40	26 04:18	5	3293

Table 2. ULTRACAM and FTN comparison stars for PG 0014+067. δ represents the brightness relative to PG 0014+067 in u', g' and r' (in magnitudes). Coordinates (J2000.0) and magnitudes from Simbad (V), the Guide Star Catalogue (C2–C4) and measured from the DSS2.J.POSS plate using ALADIN v2.5 (C5, C6, Cf).

Id	α	δ	m	$\delta u'$	$\delta g'$	$\delta r'$
PG 0014+067						
V	00 16 55.4	+07 04 32	16.5			
GSC 0000800513						
C2	00 16 54.4	+07 05 16.9	13.8	−0.74	−2.09	−2.93
GSC 0000800475						
C3	00 16 37.8	+07 03 22.6	13.6	+3.92	−2.48	−3.28
GSC 0000800043						
C4	00 16 46.4	+07 04 42.6	15.0	+0.42	−0.95	−1.73
C5	00 16 42.8	+07 02 51.5		–	+2.19	+0.98
C6	00 16 42.6	+07 06 14.4		–	+2.04	+0.31
Cf	00 16 47.5	+07 03 46.1		–	–	–

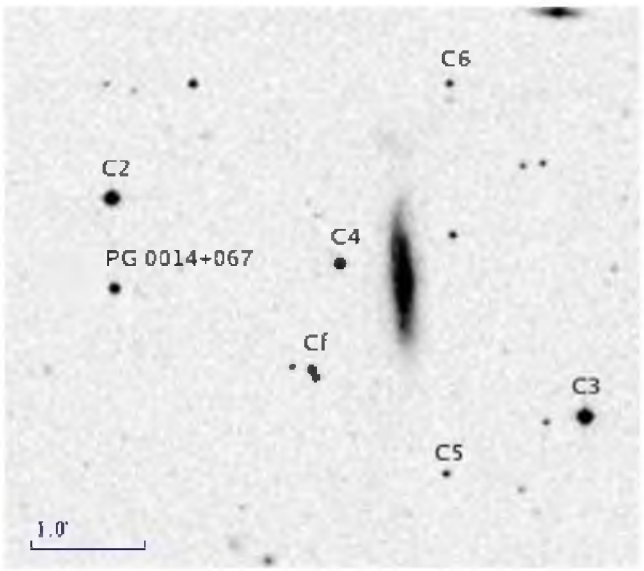

Figure 1. Chart showing the comparison stars identified in Table 2 used for ULTRACAM and FTN differential photometry (adapted from the DSS2.J.POSS plate using ALADIN v2.5 and the GIMP).

All data frames were reduced using the ULTRACAM pipeline reduction software (Dhillon et al., in preparation). Owing to changing conditions from night to night, great care was taken to select the most appropriate options offered in the reduction software. The most important choices regard the apertures used to define the star and sky. Aperture sizes may be 'fixed' or 'variable', while the extraction method may be 'normal' or 'optimal'. Because the number of target counts was always large ($\geqslant$10 000) and after checking that 'optimal' did indeed give poorer results in this high signal regime, 'normal' extraction was always used. In general, 'variable' apertures were used, because these track local changes in the seeing disc. In the case of the u' filter on nights August 22 and 23, it was found preferable to use a 'fixed' aperture, in which the star apertures and sky annuli are defined by direct examination of the raw image files. Note that 'variable' and 'fixed' refer to the sizes of the apertures; the aperture positions are updated to track image offsets from frame to frame. It was also necessary to ensure that the 'bad pixel' files used by the pipeline correctly reflected features near to any of the targets corrected by examination of the flat-fields for each night.

The star counts were combined by ratio with the comparison star, and converted to obtain a differential magnitude (V–C) in each channel. Differential magnitudes were also formed for a check star (Ck–C). To ensure the best photon statistics, the choice of comparison and check stars was not the same for each filter. The principal comparison was C4 (Table 2) in g' and r', and C2 in u'. The check star was C2 in g' and r' and C4 in u'.

All differential magnitudes from the individual ULTRACAM runs were merged into two data sets, one for each target. The data were normalized by subtracting a low-order polynomial fit to the data for each night, thus removing long-term trends including the nightly variation in differential atmospheric extinction, to give a mean value of zero in each channel. The data were cleaned by removing points lying more than $> \pm 0.1$ mag from the mean, corresponding to only 39 points in the u' filter, one in r' and none in g'.

All data frames are individually time-stamped with the Modified Julian Date (UTC; MJD = JD 240 0000.5) at the centre of the exposure. The time-stamp is obtained from typically six to seven satellites in the Global Positioning System. No correction for light travel time has been made at this stage on the bases that (i) the key thing is to have a well-understood and correct time and (ii) the consequences for frequency measurement are small for the time-base of the present observations alone.

Hence, for each principal target, differential light curves of the form (V–C) in each of u', g' and r' have been constructed, and are illustrated in Fig. 2. Differential light curves for the check star (Ck–C) have also been constructed.

Several features are immediately apparent from Fig. 2. First, the characteristic oscillations with periods of $\sim$140 s are apparent in all three filters. Secondly, beating indicates that there is more than one closely spaced frequency present. Thirdly, the variable conditions from night to night are apparent, particularly in the quality of the u' data. Notwithstanding the latter, it is clear that the amplitude of the oscillation is greatest in u'. It is also clear that the amplitude of the dominant pulsations in all three filters, and particularly in g' and r', appears to diminish between the first and the fourth night by a factor of $\sim$2 before increasing again in night 6.

2.2 Faulkes Telescope North

The Faulkes Telescope Project consists of two identical 2-m telescopes which are clones of the Liverpool Telescope (Steele 2001). The telescope sites have been chosen so that observing during the UK school day is possible. Faulkes Telescope North (FTN) is located on the mountain of Haleakala, on the Hawaiian island of Maui at an altitude of 3000 m above sea level with a mean seeing around 1 arcsec. Faulkes Telescope South is located at Siding Spring Observatory, New South Wales, Australia. Each telescope is designed for both remote and robotic operation and is equipped with a 2048^2 CCD camera with a 4.6×4.6 arcmin^2 field of view giving a pixel resolution of 0.13 arcsec.

PG 0014+067 was observed on five nights in 2004 August with the FTN in robotic mode. The CCD camera was used with a Bessell V filter and an exposure time of 15 s. Instrumental overheads for readout provided an overall cycle time of 23.25 s per exposure. A journal of FTN observations is given in Table 3. At this time, the camera could not compensate for field rotation due to the telescope motion (alt-az mounting) so repeat frames are not well aligned and could not be reduced using the ULTRACAM software.

Each of the FTN data sets was observed at a different rotator angle and with a different pointing. The observations on August 21, 24 and 25 were each interrupted once, resulting in a total of eight individual data sets. In addition to the different pointings, the tracking did not work perfectly at the time of the observations, causing a significant drift of field of view in some of the data sets.

We have reduced the FTN data with the pipeline described by Gänsicke et al. (2004). In brief, the FTN data are delivered preprocessed for bias and flat-field correction. Our software then performs aperture photometry on each image using SEXTRACTOR (Bertin & Arnouts 1996). The aperture radius was adjusted for each image to 1.5 times the median seeing computed from all the detected stars, a value that empirically results in the best signal-to-noise (S/N) ratio. The object lists produced by SEXTRACTOR were then matched by comparing the distance vectors of all possible pairs of stars. Differential light curves of PG 0014+067 were computed with respect to C2 (Table 2). As a consequence of the different pointings, not all data sets contain the same set of secondary comparison stars and different check stars had to be used, including Cf (Table 2). The timing of the individual data points was computed from the exposure

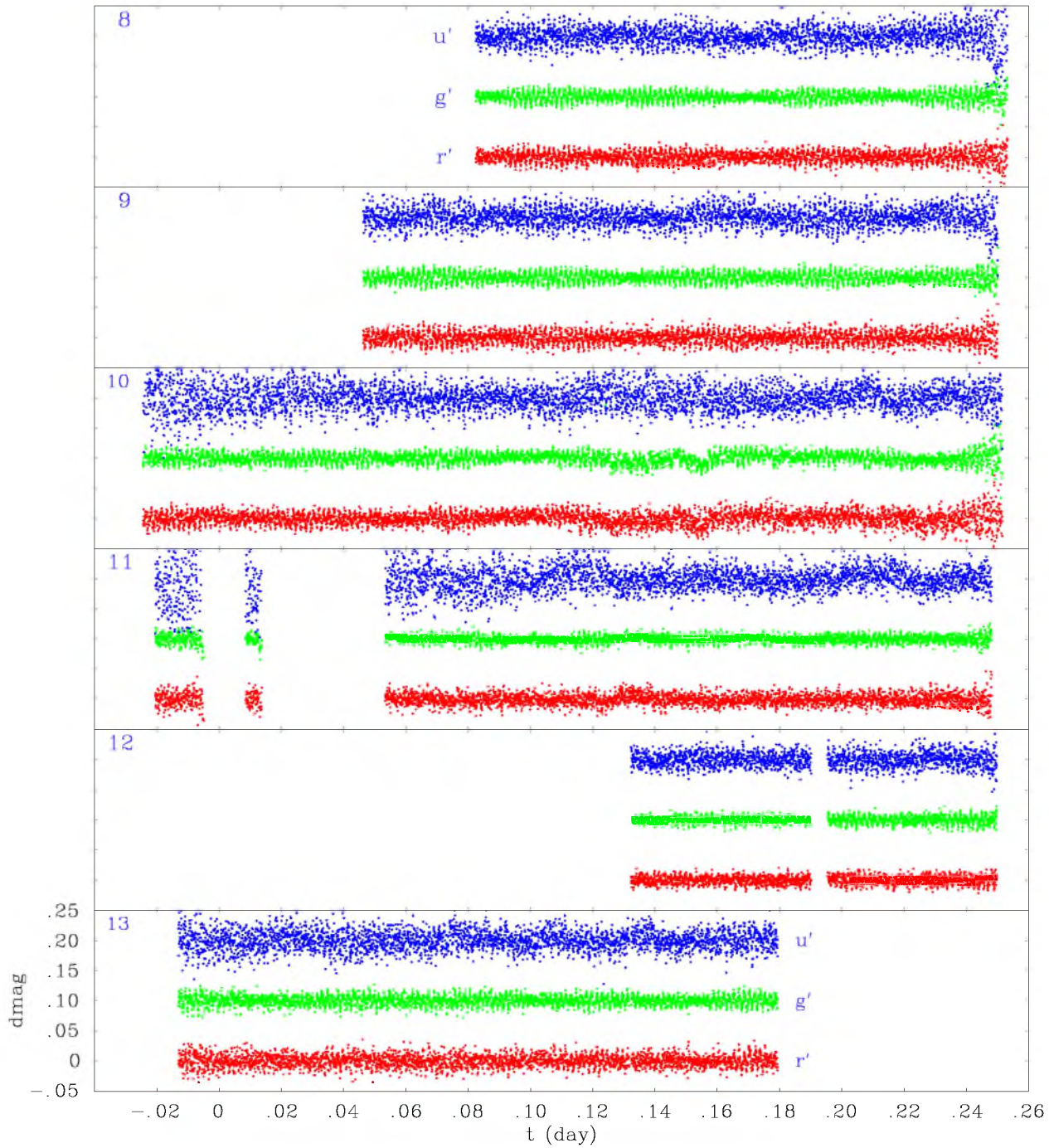

Figure 2. ULTRACAM light curve for PG 0014+067 on 2004 August 20–25 (top to bottom). The differential light curves (V–C) are shown for each filter u', g' and r' (top to bottom in each panel, labelled and, in the on-line version, coloured blue, green and red). The panels are labelled with the date of observation given as JD 245 3230. The g' and u' data are offset vertically by an arbitrary amount.

start, as given in the fits headers of the images, adding half of the exposure time, and applying the appropriate heliocentric correction.

Again, the data were normalized by subtracting a low-order polynomial fit to the data for each night, thus removing long-term trends including the nightly variation in differential atmospheric extinction, to give a mean value of zero in each channel. This also compensates for the use of different comparison stars on different nights. A plot of the light curve from one night is shown in Fig. 3. While these data are substantially noisier than the ULTRACAM data, they do contain similar periodic content. This is demonstrated in Fig. 3 by the Scargle periodogram for an individual night.

2.3 Combined data: 'white light'

In order to obtain the highest quality data set possible, the data from all three ULTRACAM channels have been combined to form a pseudo white light curve. This was achieved by forming a mean weighted by the nominal counting statistics n_k for variable and comparison

Table 3. Journal of FTN observations in 2004 August.

UT start	UT end	t_{exp}/s	n_{exp}
2004 Aug 21 13:52	21 15:25	15	240
22 09:00	22 10:33	15	240
22 11:49	22 13:22	15	240
24 12:08	24 13:15	15	172
25 08:39	25 09:29	15	130
25 12:42	25 14:14	15	240
26 08:26	26 08:59	15	84

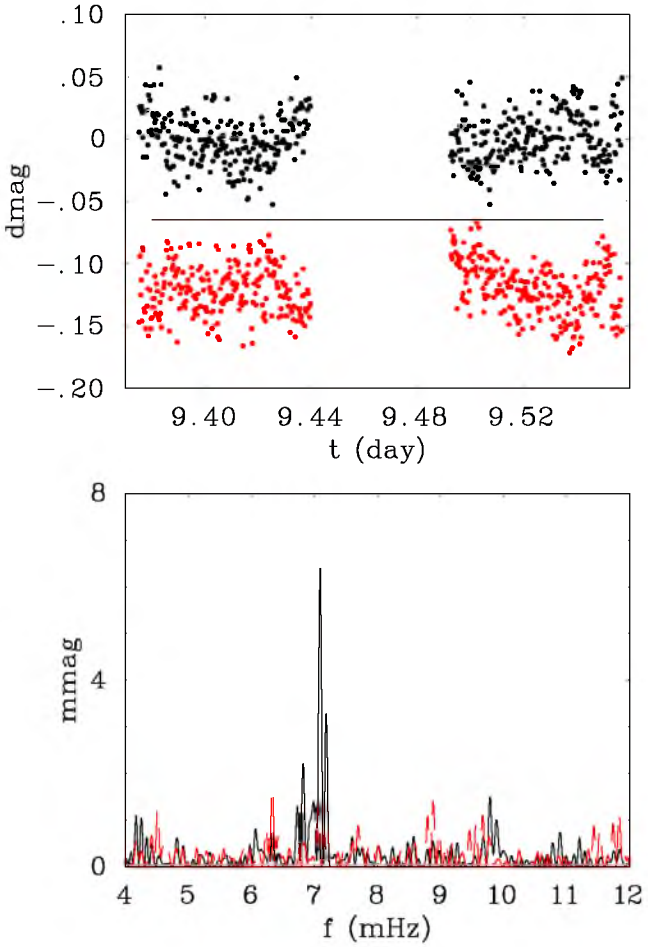

Figure 3. FTN light curve for PG 0014+067 on 2004 August 21. The differential photometry (V–C, black) and (Ck–C, grey or red) is shown in magnitudes in the upper panel, the latter offset by an arbitrary amount. Time (t) is JD 245 3230. A part of the Scargle periodograms for these data alone is shown in the lower panel for V–C (solid black) and Ck–C (broken grey or red).

stars in each channel k, i.e.

$$w_k = \left(n_{k\mathrm{V}}^{-1} + n_{k\mathrm{C}}^{-1}\right)^{-(1/2)} \quad (1)$$

resulting in relative weights of 0.39, 1.0 and 0.77 for the u', g' and r' contributions to the V–C differential light curve, respectively, and of 0.22, 1.0 and 1.05 for the Ck–C light curve. The nominal error on an individual V–C observation is 5.5 mmag, and there are some 20 056 data points in the light curve. There has been some discussion concerning the weights to be used in forming these means. One alternative would have been to use the inverse variances for the differential light curves measured in each filter. This would have given relative weights of 0.42, 1.0 and 0.80 for V–C, and 0.30, 1.0 and 0.92 for Ck–C, respectively. These are sufficiently close to the former values to have little impact on either the resulting frequencies or their relative amplitudes. Another would have been to use $w_k = (n_{k\mathrm{V}}^{-2} + n_{k\mathrm{C}}^{-2})^{-(1/2)}$, giving relative weights of 0.16, 1.0 and 0.56 in V–C resulting in the g' data dominating the overall light curve. In retrospect, the particular choice of weights was arbitrary, but provides a compromise between a photon-limited noise model and a variance model.

This ULTRACAM pseudo white light curve was then combined with 1300 data points from the FTN, resulting in a light curve spanning 5.29 d with a duty cycle of 31 per cent.

3 FREQUENCY ANALYSIS

3.1 Methods

The frequency analysis presented here assumes that the variations seen in the data comprise a multiperiodic sinusoidal oscillation. In order to identify the principal components in this oscillation, the Lomb–Scargle periodogram (LSP; Scargle 1982) has been constructed. Although the data are well sampled locally, the window function is complicated by the cycle d^{-1} alias (0.0116 mHz) and by the brevity of the time series (Fig. 4).

The procedure used to identify significant frequencies from the LSP was iterative and is illustrated in Fig. 5. First, the frequency f_i corresponding to the highest peak was measured directly from the LSP. The data were then pre-whitened by fitting a sine function at this (fixed) frequency. The amplitude a_i and phase ϕ_i of this sine function were recorded, with errors. The error on the frequency was computed from the expression given by Cuypers (1987)

$$\sigma_{f_i} = \frac{b\sigma_{\mathrm{ind}}}{\sqrt{N}a_i T} \quad (2)$$

where σ_{ind} is the average error on N independent observations, a_i is the amplitude of the signal with frequency f_i and T is the length of the time series. The value for b is still a matter of debate, but we have adopted it to be 4.9, which is conservative (see Cuypers 1987, p. 21 for a discussion).

Subsequently the LSP of the residual data was computed, the highest peak identified, its frequency measured, and the pre-whitening process repeated. In some cases, two or more well-separated frequencies would be identified and the data pre-whitened using a simultaneous fit for each sine function. This iterative process was terminated when no further frequencies could be identified with $\mathrm{S/N} > 4\sigma$, where σ is the average amplitude of the periodogram of the final residuals, computed over the frequency interval [4, 12] mHz. This stop criterion was derived empirically for δ Scuti network campaigns by Breger et al. (1993). Kuschnig et al. (1997) have shown from simulations that this criterion corresponds to a 99.9 per cent confidence limit of having detected a true frequency rather than a peak resulting from the noise. A 99 per cent confidence limit would result in the requirement $\mathrm{S/N} > 3.6\sigma$. Note that Brassard et al. (2001) have adopted the acceptance criterion $\mathrm{S/N} > 3\sigma$, which corresponds to an 80 per cent confidence limit (Kuschnig et al. 1997). We are hence far more conservative than Brassard et al. (2001) in accepting frequencies. After finalization of the frequency search, a multifrequency sine fit was made to the original data for all significant frequencies, keeping the values f_i fixed to those derived from the LSP.

The above procedure was followed for the combined 'white light'

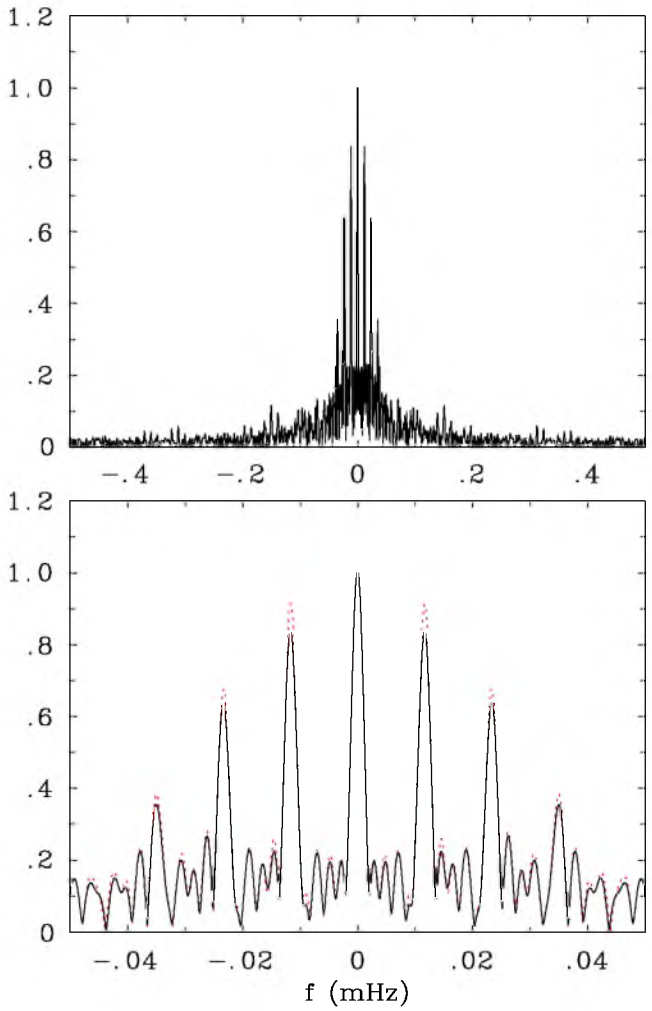

Figure 4. The window function for the combined ULTRACAM pseudo white light and FTN photometry of PG 0014+067. The lower panel also shows part of the window function for the ULTRACAM data alone (dotted grey or red).

curve and for the light curves obtained in individual ULTRACAM filters. The bottom panel in Fig. 5 shows the residual LSP over the interval [4, 12] mHz for the 'white light' data after removal of all signals given in Table 4. Furthermore, there are no peaks approaching the 4σ limit in the range [12, 23] mHz.

As an additional measure of consistency, two authors (Aerts and Jeffery) carried out the entire data reduction and analysis procedure independently. In these preliminary studies, different aperture options and different comparison stars were selected for the photometry extraction. Although one approach yielded a lower S/N light curve than that presented here, the same frequencies were obtained. Secondly, one of us carried out the frequency analysis using a number of different methods. In all cases, the top 10 frequencies identified were identical.

3.2 Solutions

The final solutions, including frequencies and amplitudes, are shown in Table 4, together with the phase shifts between signals in different filters. Table 4 also lists the frequencies and amplitudes identified by Brassard et al. (2001) and Charpinet et al. (2005a) with $a > 3\sigma$. We have identified our frequencies (to within 10 μHz) with those obtained in earlier studies wherever possible; in many cases the frequency differences correspond to a cycle d^{-1} alias. This solution is compared with two sections of the white light data in Fig. 8. The frequency solution for the combined 2004 August data is compared with the Brassard et al. (2001) and Charpinet et al. (2005a) solutions in Figs 6 and 7. These solutions provoke a number of general remarks.

(i) The amplitudes of the oscillations are strongly wavelength-dependent, being generally strongest in the ultraviolet. This is expected for non-radial oscillations in B stars, because temperature variations are the dominant cause of light variation, and these produce the largest flux changes in the ultraviolet.

(ii) The relative amplitudes of principal frequencies have altered since the measurements carried out in previous analyses (Brassard et al. 2001; Charpinet et al. 2005a). It has already been established that the amplitudes of individual modes in non-radially oscillating sdB stars vary on time-scales of days, weeks or months (cf. Kilkenny et al. 1999). The phenomenon was also reported in KPD 2109+4401 and HS 0039+4302 from ULTRACAM observations made by ourselves (Jeffery et al. 2004). The question arises as to whether this behaviour is due to a physical change in the star or to long-period beating between very closely spaced modes.

(iii) The phase difference between the light variations in u', g' and r' is almost universally smaller than 0.1 cycles. This is anticipated because, for hot stars, the variations at optical wavelength are dominated by the temperature effect (cf. Ramachandran, Jeffery & Townsend 2004).

(iv) The frequencies around 7.09 and 6.64 mHz show a multiplet-like structure, corresponding to mean splittings of ∼1.3 and 13.5 μHz, respectively (see Fig. 7). Here, the question arises as to the veracity of these multiplet structures. The spacing of the two strongest modes in the first group (2.6 μHz) is approximately $2–3\,\sigma_f$, but for the remainder σ_f is substantially larger. The spacing in the second group is close to the 11.6 μHz or 1 cycle d^{-1} alias. Brassard et al. (2001) and, subsequently, Charpinet et al. (2005a) report that up to four of their identified frequencies 'are in fact well resolved, evenly spaced multiplets with a mean frequency spacing of $\Delta f \sim 9.36$ μHz.'

(v) 13 of the frequencies identified by us (Table 4) were also identified by either Brassard et al. (2001) or Charpinet et al. (2005a) or both. Six of our frequencies have not been identified before. Three frequencies detected by both Brassard et al. (2001) and Charpinet et al. (2005a) ($a > 3\sigma$) were not seen above 4σ by us (i.e. at 6.2, 7.67 and 7.9 mHz).

3.3 Amplitude variability

It was noted above that the amplitude of the dominant mode could be seen to vary from night to night by inspection of the light curve (see Figs 2 and 8). To examine this phenomenon, the data sets were divided by night, and a two-frequency solution was computed for each night in each of the u', g' and r' filters and in the combined light curve. The amplitudes and phases for each night and for each filter are shown in Table 5, and for the combined light curve only in Figs 9 and 10.

The amplitude appears to vary sinusoidally with a period of ∼5 d. It can be explained entirely by the effect of beating between the closely spaced modes at 7.0916 and 7.089 mHz. In the multifrequency solution to the entire data set, the apparent night-to-night variation is well reproduced (Fig. 8). The frequency difference between the two principal modes contributing to the beat is 2.6 ±

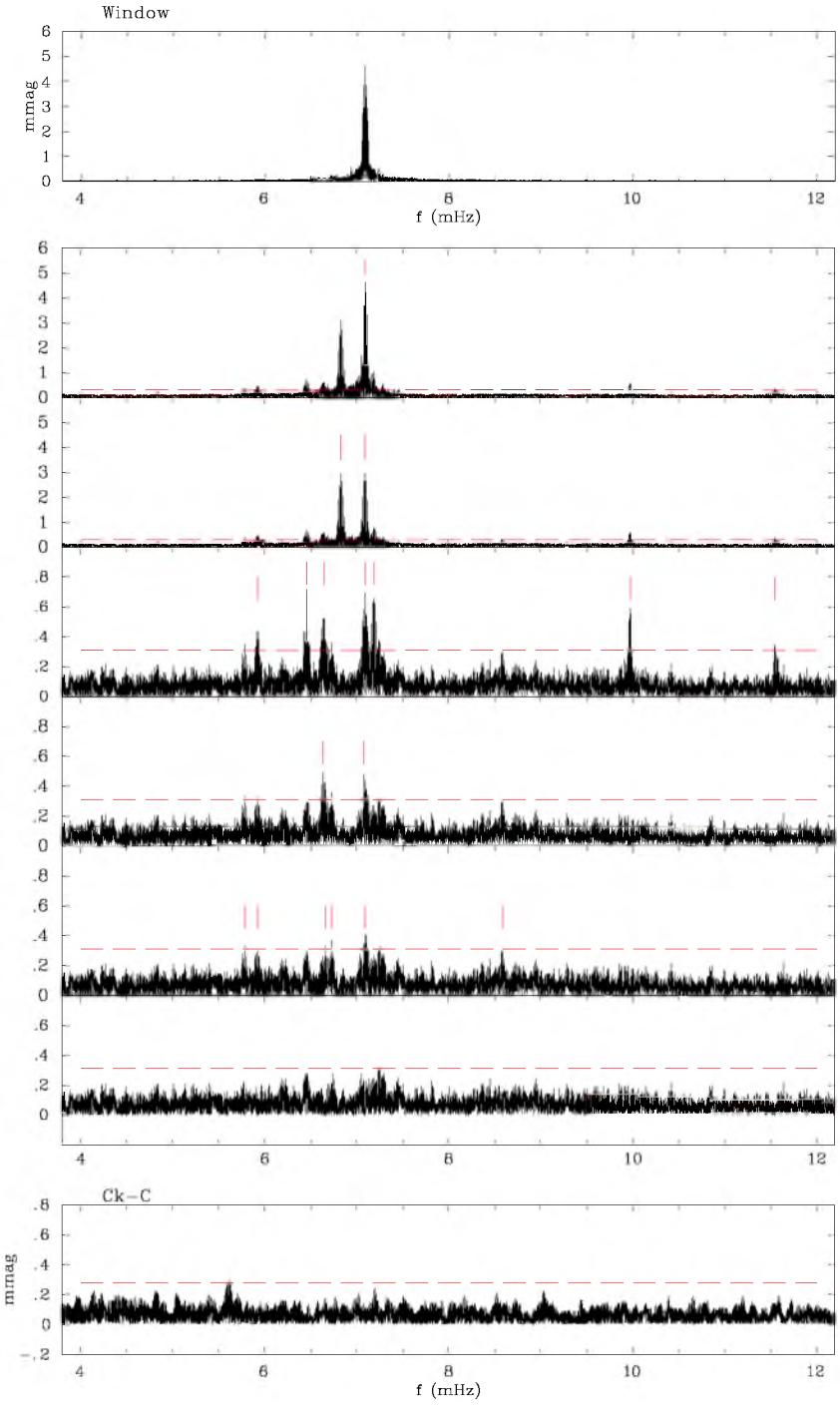

Figure 5. Periodogram analysis of the ULTRACAM light curve for PG 0014+067. The top panel shows the window function for a sinusoid sampled in the same way as the data. The second panel shows a section of the LSP for the combined ULTRACAM pseudo white light and FTN data sets. Subsequent panels show the LSPs for data successively pre-whitened by the frequencies indicated in the preceding panel. The lower panels show the 4σ threshold (dashed red/grey line) below which candidate frequencies were rejected. The bottom panel shows the LSP for the Ck–C light curve, including the 4σ threshold (dashed red/grey) for that data set.

1.2 μHz, corresponding to 4.4 ± 2.1 d. This gives substantial credence to the resolution of these two very closely spaced modes, despite the relatively short total coverage. In contrast, the isolated mode at 6.826 mHz shows less evidence for amplitude variation.

A second reason for attributing the amplitude variation to beating is the apparent phase variation. If this were due simply to amplitude modulation of a single frequency, then the phase would not vary, as seen in the 6.826-mHz mode (Fig. 10). That the 7.089-mHz mode does so on the same time-scale as the amplitude points strongly to interference between two closely spaced frequencies.

Such an interpretation for the apparent amplitude variation provides a probable explanation for the difference in amplitudes observed by us and by Brassard et al. (2001) and Charpinet et al. (2005a). With sufficient closely spaced frequencies, the instanta-

Table 4. Frequencies f, amplitudes a (mmag) and phase differences ϕ (2π radians) of periodic variations in the ULTRACAM photometry of pulsating sdB star PG 0014+067 obtained in 2004 August. f_B and a_B (per cent) are taken from table 3 of Brassard et al. (2001). f_C and a_C (per cent) are taken from table 2 of Charpinet et al. (2005a), data in angled brackets refer to evenly spaced multiplets with ~9.36 μHz spacing. Values for σ in all three 'white light' data sets and for a_w/σ in the current data are also shown. " indicates a frequency which may be present in the multiplet shown above by angled brackets.

	f/mHz	a_w	a_w/σ	$a_{u'}$	$a_{g'}$	$a_{r'}$	$\phi_{u'}-\phi_{g'}$	$\phi_{u'}-\phi_{r'}$	f_B	a_B	f_C	a_C
σ		0.0078								0.010		0.0093
f_1	5.780(9)	0.35(6)	4.5	–	–	–	–	–	–	–	5.7802	0.0423
									5.8962	0.0388		
f_2	5.921(9)	0.35(6)	4.5	0.2(2)	0.34(8)	0.5(1)	0.3(2)	0.2(2)	5.9232	0.0481	⟨5.9270⟩	⟨0.0539⟩
f_3	5.924(8)	0.40(5)	5.1	0.6(2)	0.41(7)	0.4(1)	−0.10(3)	−0.09(4)	–	–	"	"
									6.2277	0.0390	6.19373	0.0584
f_4	6.454(4)	0.71(5)	9.1	0.7(2)	0.67(6)	0.78(8)	0.03(4)	0.02(4)	–	–	⟨6.4562⟩	⟨0.1142⟩
f_5	6.632(6)	0.49(5)	6.3	0.8(1)	0.57(7)	0.6(1)	0.02(3)	0.04(3)	6.6211	0.2183	⟨6.6265⟩	⟨0.0689⟩
f_6	6.646(5)	0.60(6)	7.7	0.9(2)	0.69(7)	0.62(9)	−0.01(4)	−0.05(4)	6.6307	0.0548	"	"
f_7	6.659(9)	0.34(6)	4.3	–	–	–	–	–	–	–	"	"
f_8	6.726(8)	0.37(6)	4.7	–	–	–	–	–	–	–	–	–
f_9	6.826(1)	2.95(4)	37.7	4.0(2)	3.03(6)	2.68(8)	0.014(5)	0.015(5)	6.8375	0.1729	6.82618	0.2412
f_{10}	7.076(6)	0.50(7)	6.4	–	–	–	–	–	7.0791	0.0393	⟨7.07968⟩	⟨0.2645⟩
f_{11}	7.089(1)	2.94(6)	37.5	4.5(2)	3.20(7)	3.04(9)	0.001(7)	0.002(7)	7.0887	0.1950	"	"
f_{12}	7.0916(7)	4.60(9)	58.7	5.9(3)	5.03(9)	4.6(1)	−0.004(7)	−0.002(7)	–	–	–	–
f_{13}	7.093(4)	0.78(9)	10.0	1.2(3)	1.1(1)	1.0(1)	−0.01(4)	0.00(4)	–	–	–	–
f_{14}	7.094(8)	0.36(7)	4.6	0.5(2)	0.51(8)	0.6(1)	0.00(4)	0.03(4)	–	–	–	–
f_{15}	7.187(5)	0.66(6)	8.4	0.8(2)	0.71(8)	0.8(1)	−0.07(4)	−0.07(4)	7.1502	0.1435	7.16640	0.0808
									7.2862	0.0318	–	–
									7.6703	0.0281	7.6703	0.0284
									7.9521	0.0466	7.9283	0.0357
f_{16}	8.588(9)	0.32(6)	4.1	–	–	–	–	–	8.5521	0.0312	8.5521	0.0298
									9.7976	0.0337	–	–
f_{17}	9.971(5)	0.59(5)	7.5	0.9(2)	0.69(7)	0.6(1)	0.00(4)	−0.02(4)	9.9703	0.1061	9.9711	0.1040
f_{18}	11.547(9)	0.34(6)	4.3	0.4(2)	0.33(7)	0.37(9)	0.02(3)	−0.05(3)	–	–	–	–
									12.3868	0.0462	–	–
f_{19}	12.910(9)	0.32(5)	4.1	–	–	–	–	–	–	–		

neous appearance of the light curve can develop substantially on a time-scale of weeks. The more substantial baseline to be provided by the WET campaign will be instructive in this regard.

4 ASTEROSEISMOLOGY

The multiperiodic light variations in sdB stars are ascribed to an ensemble of non-radial oscillations, each mode of oscillation being characterized by the number of radial (k), spherical (l) and azimuthal (m) nodes. To carry out a quantitative analysis of stellar properties, it is preferable to identify, as far as possible, which oscillations correspond to which mode. If this can be achieved, then observed frequencies may be compared with the spectrum of frequencies predicted for a theoretical model of the stellar interior. Fig. 12 compares, for example, the surface properties of all three 'ULTRACAM' sdBs with evolution tracks for extreme horizontal branch stars with $M_c \approx 0.46\ M_\odot$. PG 0014+067 lies at the evolved edge of this sequence, but only part way across equivalent sequences with more massive cores. Asteroseismology can lift the degeneracy between these sequences, as amply demonstrated by Brassard et al. (2001).

4.1 Amplitude ratios

In terms of light variations, a key discriminant of the spherical degree l has been shown to be the ratio of the light amplitudes at different wavelengths (Heynderickx, Waelkens & Smeyers 1994), represented here by $a_{x'}/a_{g'}$ where $a_{x'}$ is the amplitude in filter x'. These are shown for PG 0014+067 as a function of wavelength in Fig. 11 for all frequencies where a could be measured in all three filters. Equivalent measures for a theoretical model (Ramachandran et al. 2004) are also shown.

The amplitude of the oscillation is a function of wavelength because it reflects the response of the spectrum to changes in temperature, surface gravity and radius, projected over the visible hemisphere of the star. In the case of an early-type star, the variation at u' dominates that at longer wavelengths primarily because of the effective temperature variation which affects the overall flux. This is also in phase with the variation in surface gravity which changes the Balmer decrement. Radius effects, which tend to be out of phase (by $\sim\pi$ radians) with the temperature variation, are roughly independent of wavelength for stars of this temperature. The wavelength dependence of the amplitude ratio as a function of oscillation mode is more complicated, affected by the degree of cancellation across the surface (more for higher-degree modes) and by limb-darkening, which reduces cancellation by concentrating light towards the disc centre.

In practice, for these sdB stars, the measured amplitude ratio can only distinguish between $l = 3$, $l = 4$ and $l = 0$, 1, 2, the latter three modes being essentially degenerate in this diagnostic in the adiabatic approximation. Furthermore, in the case of PG 0014+067 the formal errors in the measured amplitudes (particularly $a_{u'}$) preclude positive mode assignments. However, it is possible to argue that individual modes are unlikely to be due to a certain spherical degree. This situation occurs for the three largest-amplitude modes with frequencies f_{12}, f_9 and f_{11} (see Fig. 11). Indeed, we can

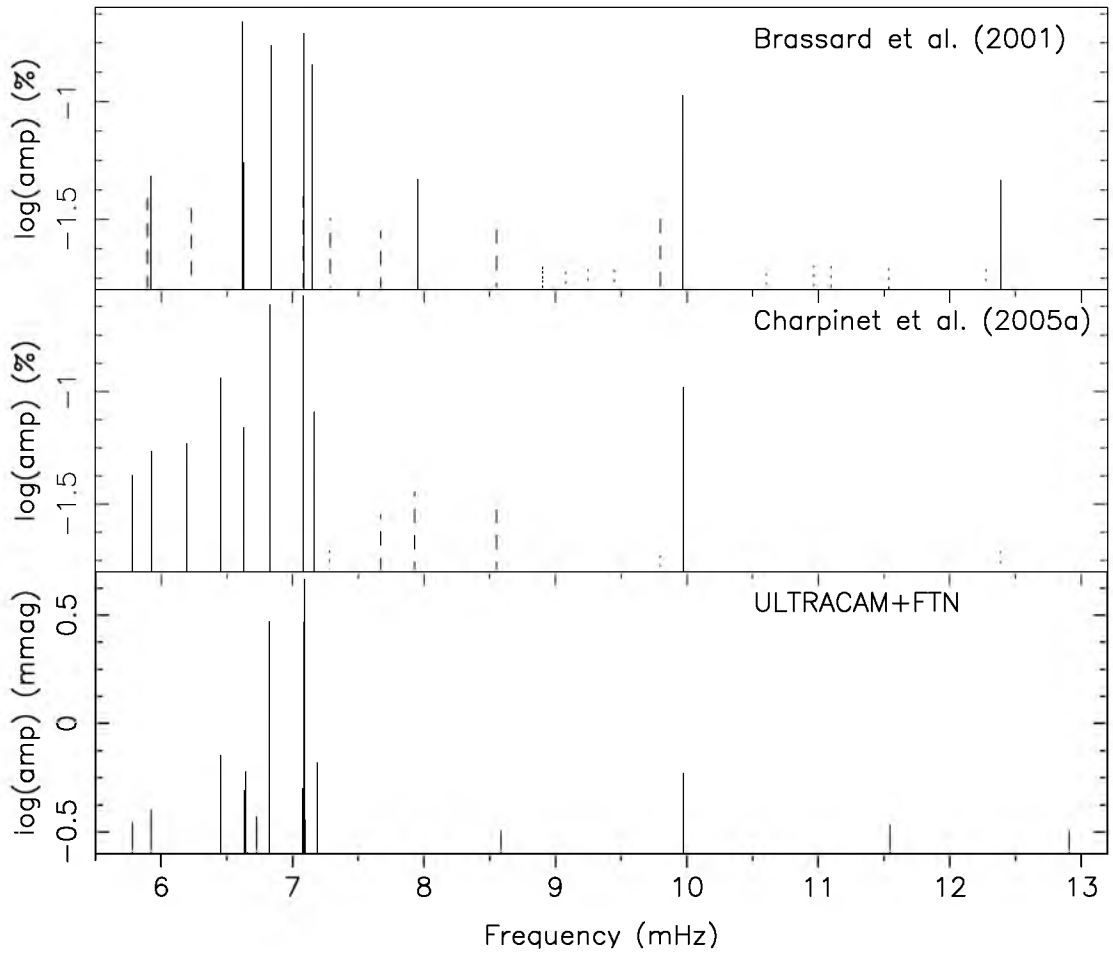

Figure 6. The frequency amplitude spectrum for the combined 2004 August data for PG 0014+067 is compared with the spectrum published by Brassard et al. (2001) (top panel) and Charpinet et al. (2005a). In the upper two panels, dashed lines refer to mode detections between 3σ and 4σ. In the top panel only, dotted lines refer to peaks in the amplitude spectrum $<3\sigma$ coincident with frequencies predicted by the Brassard et al. (2001) asteroseismic solution. All solid lines (all panels) refer to $>4\sigma$ detections.

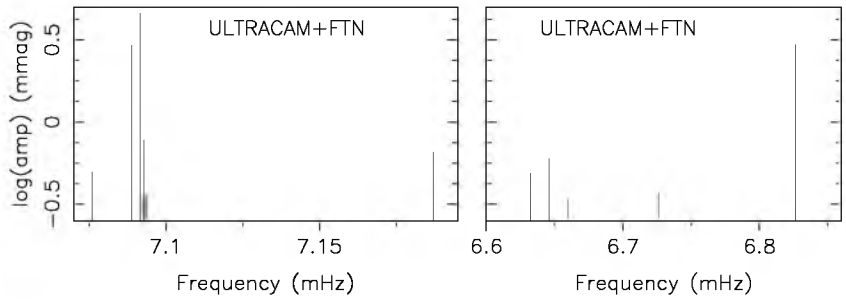

Figure 7. As Fig. 6 showing expansions around the main peaks at 7.09 and 6.65 mHz in the 2004 August data.

exclude $f_{12} = 7.0916$ mHz to be due to an $l = 3$ mode at 95 per cent confidence level. For $f_9 = 6.826$ mHz we can exclude both $l = 3$ and $l = 4$ at 95 per cent confidence level. The situation is more complex for $f_{11} = 7.089$ mHz, for which the blue amplitude ratio is compatible with $l = 0$, 1, 2, 3 but the red one only with $l = 0$, 1, 2, 4. In principle, this implies that $l = 0$, 1, 2 for this mode at 95 per cent confidence level. However, given the large uncertainty for the amplitude in the u' filter, we caution against overinterpretation. We also note that $f_{11} = 7.089$ mHz is identified as an $l = 3$ mode in the optimum solution obtained by Brassard et al. (2001). For all the additional modes, the error bars are too large to discriminate between $l = 0, \ldots, 4$. This accords with prior expectation and is not surprising because the amplitudes drop by about a factor of 4 between the three dominant modes and the minor modes (all $\lesssim$1 mmag). While we can exclude $l > 2$ for the two principal modes, this is no longer true for the lower-amplitude ones. Hence we cannot exclude the possibility that modes with $l > 2$ occur among those listed in Table 4.

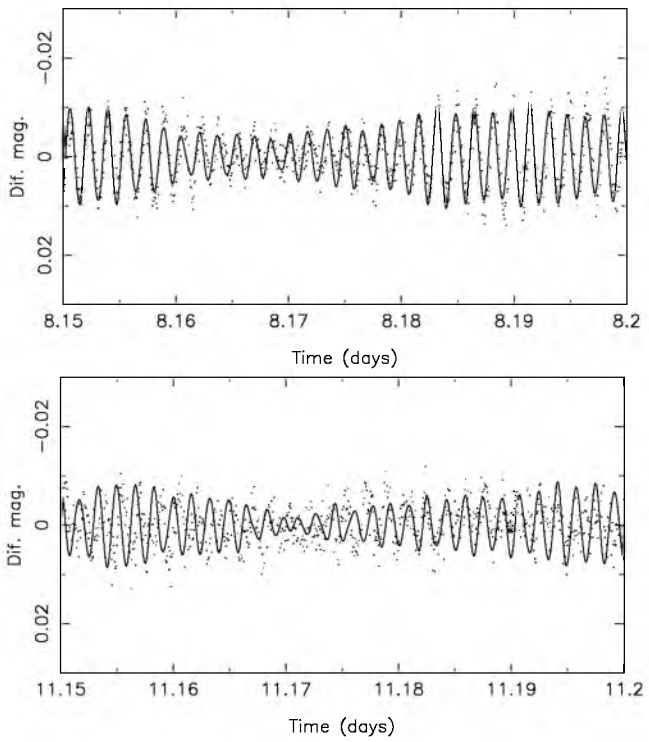

Figure 8. Two sections of the white light curve of PG 0014+067 together with the 19-frequency solution shown in Table 4. Time (t) is JD 245 3230. The change of amplitude of the dominant mode on a time-scale of days is clearly visible.

Table 5. Amplitudes (mmag) and phases (in units 2π radians) of the two dominant modes with frequencies $f_1 = 7.0916$ mHz and $f_2 = 6.826$ mHz for each night n in the 2004 August photometry of pulsating sdB star PG 0014+067. Phases were computed with respect to an arbitrary epoch.

		a_1	a_2	ϕ_1	ϕ_2
w	n_1	6.89(15)	3.13(11)	0.8901(35)	0.4986(54)
	n_2	7.45(13)	2.82(12)	0.9785(27)	0.5091(60)
	n_3	5.82(12)	3.11(10)	1.0584(15)	0.5036(47)
	n_4	1.60(15)	2.68(11)	1.0810(42)	0.4895(68)
	n_5	2.69(21)	3.07(16)	0.8397(122)	0.5163(69)
	n_6	5.13(14)	3.02(11)	0.9282(44)	0.5101(52)
u'	n_1	9.26(48)	4.37(34)	0.8813(82)	0.4972(125)
	n_2	10.16(33)	3.69(34)	0.9787(51)	0.5260(104)
	n_3	7.12(49)	4.28(44)	1.0686(41)	0.5343(105)
	n_4	1.83(63)	3.48(11)	1.1238(04)	0.4938(211)
	n_5	3.91(46)	4.43(38)	0.8089(188)	0.5118(118)
	n_6	6.97(49)	4.18(41)	0.9173(112)	0.5266(112)
g'	n_1	7.26(18)	3.32(13)	0.8895(39)	0.5028(60)
	n_2	8.22(13)	2.92(11)	0.9763(25)	0.5009(62)
	n_3	5.75(17)	3.04(13)	1.0593(21)	0.4981(70)
	n_4	1.76(17)	2.93(13)	1.0697(56)	0.5014(69)
	n_5	3.29(23)	3.34(18)	0.8342(109)	0.5163(70)
	n_6	5.16(21)	2.96(16)	0.9319(64)	0.5042(83)
r'	n_1	6.77(25)	2.59(18)	0.8860(60)	0.4988(111)
	n_2	7.28(20)	2.81(19)	0.9814(44)	0.5055(100)
	n_3	5.55(24)	2.73(20)	1.0542(33)	0.4907(115)
	n_4	1.35(28)	2.31(20)	1.0957(61)	0.5027(135)
	n_5	2.74(27)	3.23(22)	0.8332(156)	0.5240(82)
	n_6	4.78(29)	2.81(22)	0.9309(95)	0.5002(122)

Table 6. Frequency resolution of data sets. Bra01 denotes Brassard et al. (2001) and Cha05 denotes Charpinet et al. (2005a).

	Bra01	Cha05	Current ULTRACAM	Current All
T/d	4.07	4.09	5.11	5.31
$1/T/(\mu\text{Hz})$	2.84	2.82	2.26	2.18
$1.5/T$	4.26	4.24	3.39	3.27
$2.5/T$	7.11	7.07	5.66	5.45

4.2 Multiplicity

A clear consequence of both the current results and those of Brassard et al. (2001) and Charpinet et al. (2005a) is that there are several groups of closely spaced frequencies. For example, our data (Table 4) show a pair of frequencies at f_2, f_3 separated by $\sim$3 μHz, a triplet at f_5, f_6, f_7 separated by 13.5 μHz and another triplet at f_{11}, f_{12}, f_{13} separated by $\sim$2 μHz, with f_{10} and f_{14} only 13 and 1 μHz away, respectively,

Brassard et al. (2001) reported possible multiplet structures at 7.08, 6.63 and 5.90 mHz, with spacings of 9.6, 9.6 and 27.0 μHz, respectively, while Charpinet et al. (2005a) identify evenly spaced multiplets corresponding to those identified by us, as well as at f_4, with a mean spacing $\Delta f \sim 9.36$ μHz.

It has been established that the p-mode oscillations typical of the pulsating sdB stars are of low radial order. As is well known from asymptotic analyses of the stellar oscillation equations, a characteristic frequency spacing occurs only for high-order p modes with the same low degree and with subsequent values of the radial order. Therefore, we do not expect to find such a uniform frequency spacing in PG 0014+067. However, the frequencies cannot be crowded together closely either, and, in general, will be spaced by $\sim$1 mHz (cf. Charpinet et al. 2002). Let us suppose that the multiplets identified above comprise spherical harmonics with the same wavenumbers k and l, and that rotation has broken the frequency degeneracy of modes with different m. There are then from eight to 10 independent frequencies between 5.7 and 7.2 mHz, depending on how f_{10} and f_{14} are related to the $f_{11,12,13}$ triplet. With 1-mHz spacings, this space is large enough for only two modes of a given l, or by including modes with $l = 0, \ldots, 4$, up to approximately 10 modes. Under the same supposition, the multiplets cannot, of course, be due to $l = 0$ modes.

4.3 Rotation

Assuming that the spacings of 9.6, 9.6 and 27.0 μHz are due to rotational splitting and realizing that the likely modes demand an approximately constant common spacing between adjacent m components, Brassard et al. (2001) determine a mean value $\Delta f \approx 9.5 \pm 0.3$ μHz and an estimate for the rotational period of $P_{\rm rot} \approx (\Delta f)^{-1} = 29.2 \pm 0.9$ h.

The smallest reliable frequency spacing found by us is $\Delta f = 2.6 \pm 1.2$ μHz (see Section 3.3). For uniform rotation, frequency spacings are related to the rotation frequency $\Omega/m = -\Delta f/(1 - c_{kl})$, where c_{kl} depends on the structure of the star and is normally less than unity. Values given by Charpinet et al. (2002) range between 0 and 0.2 for p modes of interest. For $\Delta f = 2.6$ μHz, $\delta m = 1$, and assuming the same l for f_{11} and f_{12}, the resulting Ω corresponds to a rotation period ($P_{\rm rot}$) between 3.6 d ($c_{kl} = 0.2$) and 4.5 d ($c_{kl} = 0$) with a mean value around 4.2 d ($c_{kl} = 0.05$).

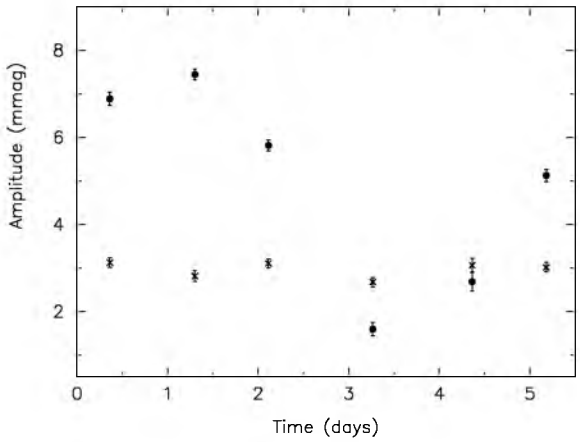

Figure 9. The amplitude in white light of the dominant modes at 7.089 mHz (filled circles) and 6.826 mHz (crosses) in the 2004 combined data set for each night (JD 245 3238).

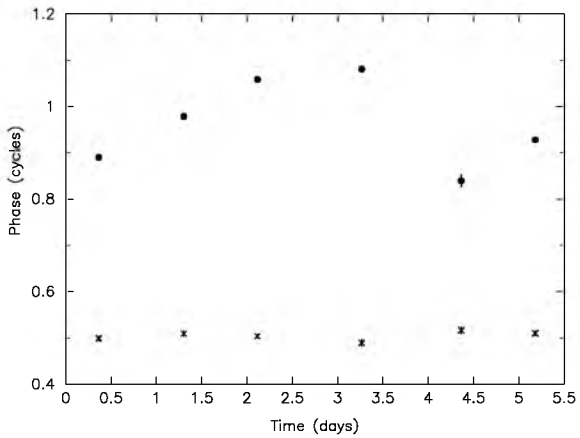

Figure 10. The phase (in units of 2π radians) in white light of the dominant modes at 7.089 mHz (filled circles) and 6.826 mHz (crosses) in the 2004 combined data set for each night (JD 245 3238). Most error bars are smaller than the plot symbols.

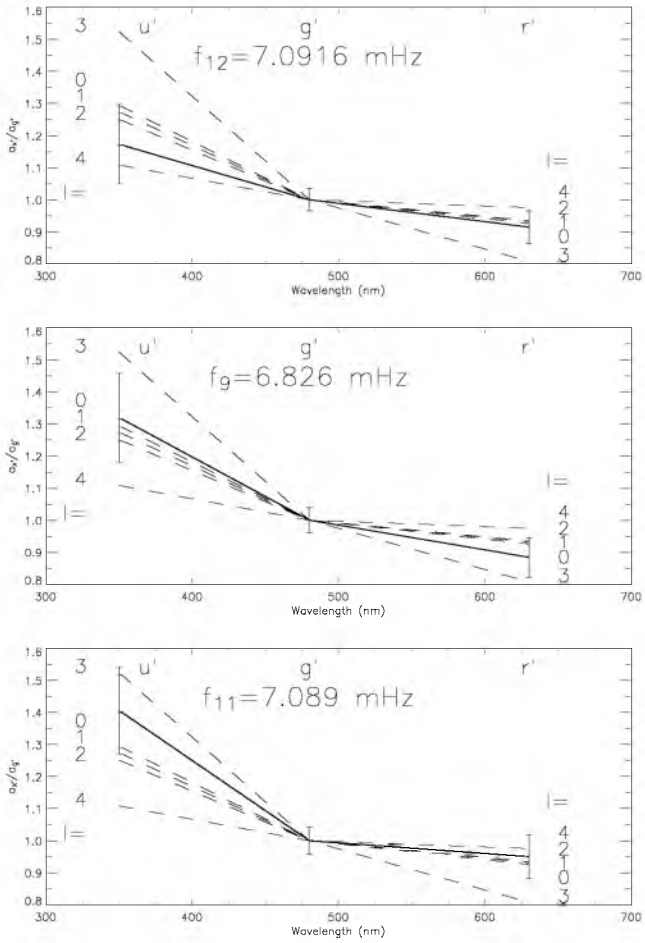

Figure 11. Amplitude ratios $a_{x'}/a_{g'}$ are shown for the three largest amplitude modes in PG 0014+067 (solid lines) together with theoretical values for a model with $M = 0.5\,\mathrm{M}_{\odot}$, $T_{\mathrm{eff}} = 32\,000$ K, $\log g = 5.8$, $f = 5.4$ mHz and for $l = 0, \ldots, 4$ (from Ramachandran et al. 2004). The error bars represent 95 per cent confidence limits.

Is this value correct? Brassard et al. (2001) and Charpinet et al. (2005a) deduce P_{rot} nearer to 29.9 h from the mean frequency spacing at 9.36 μHz. Why were these spacings not found in our data? It is instructive that the spacing of our $f_{5,6,7}$ multiplet (13.5 μHz) is exactly half the spacing of the multiplet at 5.90 mHz reported by Brassard et al. (2001). Moreover, it is roughly 2 μHz greater than the 11.57-μHz cycle d^{-1} alias. Similarly, the 9.36-μHz spacing of Charpinet et al. (2005a) is ∼2 μHz smaller than this alias. It therefore seems possible that, given the window function of both previous sets of observations, the true rotation period is nearer to 5 d. Indeed, the window function for the current data is only marginally better, and the true spacing can only be resolved for the principal peaks.

Cuypers (1987) writes that 'Loumos & Deeming (1978) concluded that frequencies with $\Delta f < 1/T$ are never found separated in the periodogram. When $1/T < \Delta f < 1.5/T$, the frequencies are separated, but the periodogram maxima do not necessary occur at the real frequencies. If $1.5/T < \Delta f < 2.5/T$, the deviations from the real frequencies become of the order of the errors on the frequencies. As soon as $\Delta f > 2.5/T$ the differences between the peak frequencies and the real frequencies become negligible, because the first negative sidelobe of the sinc function no longer interferes with the main peak of the other sinc function.' For the data presented by Charpinet et al. (2005a), $1/T = 2.82$ μHz so that the accuracy they assumed for their listed frequencies is overly optimistic. For our ULTRACAM data alone, $1/T = 2.263$ μHz. Technically $1/T = 2.180$ μHz for the full data set, but the longer baseline is provided by only 0.5 h of FTN data. Thus, $\Delta f = 2.6$ μHz is on the cusp of detectability in our data, and the maxima do not necessarily occur at the correct frequencies. Nevertheless, there seems to be good evidence for frequency splitting at a level much smaller than that seen previously. Again, the WET data will be instructive here, given that their total time base will be about twice that of our data.

5 CONCLUSION

The contributions made by previous observers of PG 0014+067 (Brassard et al. 2001; Charpinet et al. 2005a) have had a major impact because excellent data have been combined with a thorough frequency analysis and the results have been compared in detail with a superb set of theoretical models. It is also true that stellar parameters deduced from pulsation periods are remarkably robust, because the periods of low-k and low-l modes so strongly constrain the stellar radius. Therefore, new studies seem unlikely to modify these early results in any significant way. In any case, the present

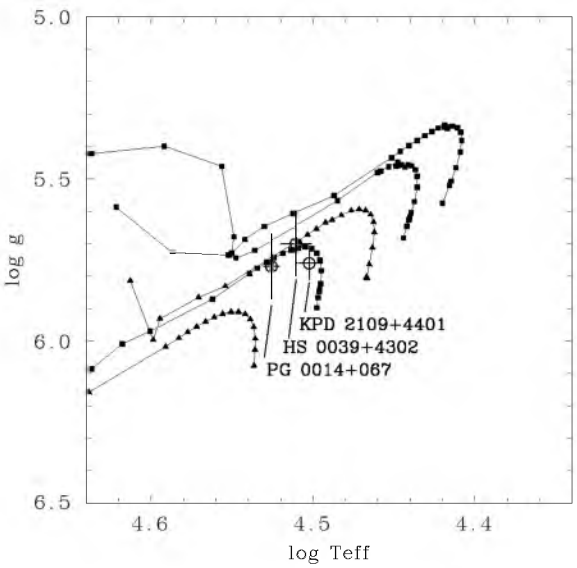

Figure 12. A g–$T_{\rm eff}$ diagram showing the locations of PG 0014+067 and both other sdBs observed with ULTRACAM (open circles with error bars; Heber, Reid & Werner 2000b; Edelmann et al. 2003; Charpinet et al. 2005a) compared with evolutionary tracks for extreme horizontal branch stars having a core mass 0.4758 $M_{\odot}$ (squares) or 0.4690 $M_{\odot}$ (triangles) and envelope masses 0.0001, 0.0002, 0.0007, 0.0012 and 0.0022 $M_{\odot}$ (left to right) (from Charpinet et al. 2002).

authors are not in a position to make a more detailed asteroseismological study. Their observations were obtained principally to identify the strongest oscillation modes using the colour–amplitude ratio method.

The combination of the WHT and ULTRACAM has proven itself to be ideally matched to the measurement of multicolour light curves for the short-period pulsating sdB stars, or EC 14026 variables. Limited only by the time allocated on the telescope, which has a corresponding impact on frequency resolution, the light curve of PG 0014+067 has been decomposed to give frequencies, amplitudes and phases for a total of 19 individual frequencies with a high degree of confidence ($>4\sigma$).

On this occasion, the magnitude of the target and the amplitude of the pulsations have combined to defeat any unequivocal identification of non-radial modes using the amplitude–ratio method. We do find that the two strongest modes cannot be modes of $l = 3$ or $l = 4$ and must be one of $l = 0$, 1, 2. The frequency resolution (which varies as $1/T$) imposed by the temporal window has also partially limited a complete decomposition of the light curve.

Assuming the close frequency spacing of 2.6 μHz to be due to the same l, and rigid rotation, we find a rotational period of ~4 d, about three times longer than previously obtained. Frequency splitting detected in other multiplets by previous authors is confirmed by us, but the measured values may be aliases of the true values. With improved frequency resolution, this rotational splitting should be measured with improved confidence.

It is appropriate to suggest what else further studies should aim to achieve. First of all, the matching of observed and theoretically predicted frequencies must consider non-radial modes with $l = 0, \ldots, 4$. The omission of $l = 4$ modes in earlier work overly restricts the parameter space in which an optimum solution may be found. If $l = 3$ modes are detected, then $l = 4$ modes are also likely to be visible. Moreover, we believe it is necessary to consider a family of acceptable models when making seismic inferences. Indeed, rather than restricting the solution to a single overall best model based on a χ^2-type argument, it is necessary to compare the detailed structure of different models that lead to almost equally good fits in order to decide whether or not seismic sounding of the interior is useful for the improvement of the input physics of the models. The observational results presented here, combined with those of twice their frequency resolution expected from the WET campaign, will hopefully lead to new efforts to model the internal structure of PG 0014+067 under various assumptions and to test these using the tools of asteroseismology.

ACKNOWLEDGMENTS

Research at the Armagh Observatory is funded by the Northern Ireland Department of Culture, Arts and Leisure and by UK Particle Physics and Astronomy Research Council (PPARC) grant PPA/G/S/2002/00546. ULTRACAM operations are currently funded by PPARC under grant PPA/G/S/2002/00092. BTG acknowledges support from a PPARC Advanced Fellowship. CA is supported by the 'Stichting Nijmeegs Universiteits Fonds' and by NOVA. The authors are particularly grateful for support at the telescope provided by the ULTRACAM team from Sheffield. They are also grateful to the Faulkes Telescope management and operations teams for making time available and for ensuring observations were made successfully. This research has made use of the SIMBAD data base, operated at CDS, Strasbourg, France.

REFERENCES

Balona L. A., Dziembowski W. A., 1999, MNRAS, 309, 221
Bertin E., Arnouts S., 1996, A&AS, 117, 393
Billères M., Fontaine G., Brassard P., Charpinet S., Liebert J., Saffer R. A., 2000, ApJ, 530, 441
Brassard P., Fontaine G., Billères M., Charpinet S., Liebert J., Saffer R. A., 2001, ApJ, 563, 1013
Breger M. et al., 1993, A&A, 271, 482
Charpinet S., Fontaine G., Brassard P., Dorman B., 1996, ApJ, 471, L103
Charpinet S., Fontaine G., Brassard P., Chayer P., Rogers F. J., Iglesias C. A., Dorman B., 1997, ApJ, 483, L123
Charpinet S., Fontaine G., Brassard P., Dorman B., 2002, ApJS, 140, 469
Charpinet S., Fontaine G., Brassard P., Green E. M., Chayer P., 2005a, ASP Conf. Ser. Astron. Soc. Pac., San Francisco, in press
Charpinet S., Fontaine G., Brassard P., Green E. M., Chayer P., 2005b, ASP Conf. Ser. Astron. Soc. Pac., San Francisco, in press
Charpinet S., Fontaine G., Brassard P., Green E. M., Chayer P., 2005c, A&A, 437, 575
Cuypers J., 1987, The Period Analysis of Variable Stars, Vol. 49, No. 3. Academiae Analecta, Royal Academy of Sciences, Belgium
D'Cruz N. L. et al., 2000, ApJ, 530, 352
Edelmann H., Heber U., Hagen H.-J., Lemke M., Dreizler S., Napiwotzki R., Engels D., 2003, A&A, 400, 939
Fukugita M., Ichikawa T., Gunn J. E., Doi M., 1996, AJ, 111, 1748
Gänsicke B. T., Araujo-Betancor S., Hagen H.-J., Harlaftis E., Kitsionas S., Dreizler S., Engels D., 2004, A&A, 418, 270
Han Z., Podziadlowski Ph., Maxted P. F. L., Marsh T. R., Ivanova N., 2002, MNRAS, 336, 449
Han Z., Podziadlowski Ph., Maxted P. F. L., Marsh T. R., 2003, MNRAS, 341, 669
Heber U., 1986, A&A, 155, 33
Heber U., Reid I. N., Werner K., 2000a, A&A, 348, L25
Heber U., Reid I. N., Werner K., 2000b, A&A, 363, 198
Heynderickx D., Waelkens C., Smeyers P., 1994, A&AS, 105, 447
Jeffery C. S., Pollacco D., 2000, MNRAS, 318, 974
Jeffery C. S., Dhillon V. S., Marsh T. R., Ramachandran B., 2004, MNRAS, 352, 699

Kawaler S., Hostler S., 2004, ApSS, 291, 387
Kawaler S., Hostler S., 2005, ApJ, 621, 432
Kilkenny D., Koen C., O'Donoghue D., Stobie R. S., 1997, MNRAS, 285, 640
Kilkenny D. et al., 1999, MNRAS, 303, 525
Kilkenny D. et al., 2002, MNRAS, 331, 399
Kilkenny D. et al., 2003, MNRAS, 345, 834
Koen C., 1998, MNRAS, 300, 567
Kuschnig R., Weiss W. W., Gruber R., Bely P. Y., Jenkner H., 1997, A&A, 328, 544
Loumos G. L., Deeming T. J., 1978, ApSS, 56, 285
O'Leary A., 2004, Observation of the binary star NN Ser using the Faulkes Telescope, Nuffield Science Bursary Project Report
O'Toole S. J. et al., 2000, ApJ, 537, L53
O'Toole S. J., Jørgensen M. S., Kjeldsen H., Bedding T. R., Dall T. H., Heber U., 2003, MNRAS, 340, 856
Quinn C., 2004, Asteroseismology of pulsating star KPD 1930+2752, Nuffield Science Bursary Project Report
Ramachandran B., Jeffery C. S., Townsend, R. H. D., 2004, A&A, 428, 209
Scargle J. D., 1982, ApJ, 263, 835
Sills A., Pinsonneault M., 2000, ApJ, 540, 489
Steele I. A., 2001, NewAR, 45, 45

This paper has been typeset from a TEX/LATEX file prepared by the author.